Acta Pharmaceutica Sinica B 2024;14(2):781−794

Chinese Pharmaceutical Association
Institute of Materia Medica, Chinese Academy of Medical Sciences

Acta Pharmaceutica Sinica B

www.elsevier.com/locate/apsb
www.sciencedirect.com

ORIGINAL ARTICLE

pH-Responsive polymer boosts cytosolic siRNA release for retinal neovascularization therapy

Shuai Guo[a,†], Chunhui Li[a,†], Changrong Wang[b], Xiaowen Cao[c], Xinyue Liu[a], Xing-Jie Liang[d], Yuanyu Huang[a], Yuhua Weng[a,*]

[a]*School of Medical Technology, Advanced Research Institute of Multidisciplinary Science, School of Life Science, Key Laboratory of Molecular Medicine and Biotherapy, Key Laboratory of Medical Molecule Science and Pharmaceutics Engineering, Beijing Institute of Technology, Beijing 100081, China*
[b]*School of Pharmacy, Shandong New Drug Loading & Release Technology and Preparation Engineering Laboratory, Binzhou Medical University, Yantai 264003, China*
[c]*School of Ophthalmology and Optometry, School of Biomedical Engineering, The Eye Hospital, Wenzhou Medical University, Wenzhou 325027, China*
[d]*Chinese Academy of Sciences (CAS), Key Laboratory for Biomedical Effects of Nanomaterials and Nanosafety, CAS Center for Excellence in Nanoscience, National Center for Nanoscience and Technology of China, Beijing 100190, China*

Received 25 June 2023; received in revised form 25 July 2023; accepted 10 August 2023

KEY WORDS

siRNA;
Ocular delivery system;
Block polymer;
Endosomal escape;
Retinal neovascularization;
Blood−retinal barrier;
VEGFA;
Safety

Abstract Small interfering RNA (siRNA) has a promising future in the treatment of ocular diseases due to its high efficiency, specificity, and low toxicity in inhibiting the expression of target genes and proteins. However, due to the unique anatomical structure of the eye and various barriers, delivering nucleic acids to the retina remains a significant challenge. In this study, we rationally design PACD, an A-B-C type non-viral vector copolymer composed of a hydrophilic PEG block (A), a siRNA binding block (B) and a pH-responsive block (C). PACDs can self-assemble into nanosized polymeric micelles that compact siRNAs into polyplexes through simple mixing. By evaluating its pH-responsive activity, gene silencing efficiency in retinal cells, intraocular distribution, and anti-angiogenesis therapy in a mouse model of hypoxia-induced angiogenesis, we demonstrate the efficiency and safety of PACD in delivering siRNA in the retina. We are surprised to discover that, the PACD/siRNA polyplexes exhibit remarkable intracellular endosomal escape efficiency, excellent gene silencing, and inhibit retinal angiogenesis. Our study provides design guidance for developing efficient nonviral ocular nucleic acid delivery systems.

*Corresponding author.
E-mail address: wengyh@bit.edu.cn (Yuhua Weng).
[†]These authors made equal contributions to this work.
Peer review under the responsibility of Chinese Pharmaceutical Association and Institute of Materia Medica, Chinese Academy of Medical Sciences.

https://doi.org/10.1016/j.apsb.2023.09.001

1. Introduction

Ocular neovascularization is associated with a variety of ocular diseases, including age-related macular degeneration (AMD), proliferative diabetic retinopathy (PDR), retinopathy of prematurity (ROP), retinitis pigmentosa (RP), etc. Loss of vision may occur if not properly controlled. Vascular endothelial growth factor (VEGF) plays a key role in the formation of new vessels, which grow from pre-existing vessels, leading to retinal edema, vascular leakage, etc[1]. The emergence of anti-VEGF antibodies such as ranibizumab, bevacizumab, or VEGF receptor antibodies (such as aflibercept) has now led to significant advances in the clinical treatment of retinal neovascularization and exudative diseases. However, patients still face frequent, repetitive injections over time to maintain the therapeutic effect[2]. RNA interference (RNAi) is an extremely specific method to inhibit pathogenic gene and protein expression[3]. In the latest 5 years, at least 5 siRNA therapeutics (Onpattro, Givlaari, Oxlumo, Leqvio, Amvuttra) have been approved by the U.S. Food and Drug Administration (FDA). Notably, a single injection of Leqvio induced a more than 50% reduction of bad cholesterol (LDL-C) levels over 180 days in patients with atherosclerotic cardiovascular disease, indicating excellent stability and efficacy of siRNA, according to data published by Leqvio[4]. In addition to clinically available anti-VEGF antibodies and small molecule drugs, siRNA is another attractive drug candidate for ophthalmic neovascular diseases because siRNA based on complementary gene sequence pairing can be designed and screened within a few days, and various chemical modifications can be introduced to siRNA to ensure long-lasting stability and efficacy[5]. Besides, the unique and relatively closed anatomy of the eye insulates the systemic circulation, making it an ideal target for nucleic acid drugs.

Although ophthalmic diseases are an important direction of nucleic acid drug development, the distribution of nucleic acid in the posterior segment of the eye still faces many challenges. For example, the blood−retinal barrier (BRB) limits drug transportation through the intraocular tissues, the small volume of intravitreal injections limits the dose given, the gelatinous vitreous body affects the rate of diffusion of different drugs, as well as some ocular administration routes are highly technical (*e.g.*, subretinal injections)[6,7]. In addition to the intraocular barrier, nucleic acids still face their common delivery issue. Since most siRNA delivery systems enter cells *via* endocytosis, they readily aggregate and degrade in the lysosomes. Even for lipid nanoparticles that are widely used clinically, the cellular escape efficiency of siRNA is reported to be less than 5%[8]. As a result, considering the high demand for ophthalmic nucleic acid therapy, there is an urgent need to develop an efficient and safe delivery system for ocular purposes.

Polymers, especially pH-responsive block copolymers, have long been pursued by researchers because of their excellent nucleic acid delivery efficiency, predictable structure and degradable properties, etc[9,10]. Similar to cationic lipids, pH-responsive polymers can be designed to be protonated and positively charged in acidic environments such as endosomes or lysosomes. They can promote endosomal escape, primarily through the proton sponge effect[11,12]. Compared with lipid nanoparticles containing at least three different kinds of lipids, copolymers, especially amphiphilic copolymers are friendly to scale production. They can self-assemble into vesicle-structured nanomicelles, which can load nucleic acids by simple mixing.

Here, we rationally designed a pH-responsive triblock copolymer **P**EG-*b*-P**A**MA-*b*-P(**C**7A-r-**D**BA) (PACD) that exhibits robust endosomal escape when delivering siRNA into retinal multilayer cells. Excellent gene silencing efficiency and long intraocular retention time were achieved (Fig. 1). The characteristics, siRNA binding capacity, gene silencing and endosomal escape mechanisms were fully evaluated. The applicability of PACD polymeric micelles for intraocular delivery of siRNA and its therapeutic effect in oxygen-induced retinopathy (OIR) mice models were also confirmed. The copolymer designed in our work overcomes some of the vital problems of nucleic acids delivery in the eye, such as intraocular clearance systems, and endosomal escape, and therefore has important significance for the development of ocular non-viral gene delivery systems.

2. Materials and methods

2.1. Materials, cells and animals

siRNAs and primers were synthesized by BIOSYNTECH Co., Ltd. (Suzhou Ribo Life Science, Suzhou, China). Lysotracker green DND-26 (Sigma Aldrich, St. Louis, MO, USA), lipofectamine 2000 (Thermo Fisher Scientific, Waltham, USA), Dulbecco's modified Eagle's medium (DMEM), DMEM/F12, Opti-MEM, fetal bovine serum (FBS), penicillin-streptomycin, gentamicin and 0.25% trypsin-ethylenediaminetetraacetic acid (EDTA) were provided by Thermo Fisher Scientific (Waltham, USA). VEGFA antibody was purchased from Abcam. The Trizol reagent was provided by Vazyme Co., Ltd. (Nanjing, China). RNA later, dimethyl sulfoxide (DMSO), 2-aminoethanol, methoxy poly (ethylene glycol) ($mPEG_{2k}$), di-*tert*-butyl decarbonate (Boc), 2 (hexamethylenediamine) ethanol (C7A), and azobisisobutyronitrile (AIBN) were purchased from Sigma−Aldrich (St. Louis, MO, USA). Endothelial cell medium was purchased from ScienCell Research Laboratories (catalog #1001, Carlsbad, CA, USA). ARPE-19 cells were a kind gift from Prof. Nan Kaihui of Wenzhou Medical University. The cells were cultured in DMEM/F12 medium supplemented with 10% FBS and 1% penicillin-streptomycin. Primary human umbilical cord blood endothelial cells (HUVECs) were isolated from human umbilical cord waste. In short, fresh human umbilical cords were washed several times in PBS buffer containing 400 U/mL gentamicin. Subsequently, the umbilical cords were cut into short pieces, infused with 0.5% trypsin, and digested at 37 °C for 1 h. Then, stop digestion with a complete medium, wash the interior several times, and collect the HUVEC cells. The cells were cultured in an endothelial cell medium. All cells were maintained at 37 °C under a 5% CO_2 atmosphere. C57BL/6J mice aged 6−8 weeks and pregnant mice aged 16−18 days were purchased from JieSiJie Experimental Animals Co., Ltd. (Shanghai, China). All animal

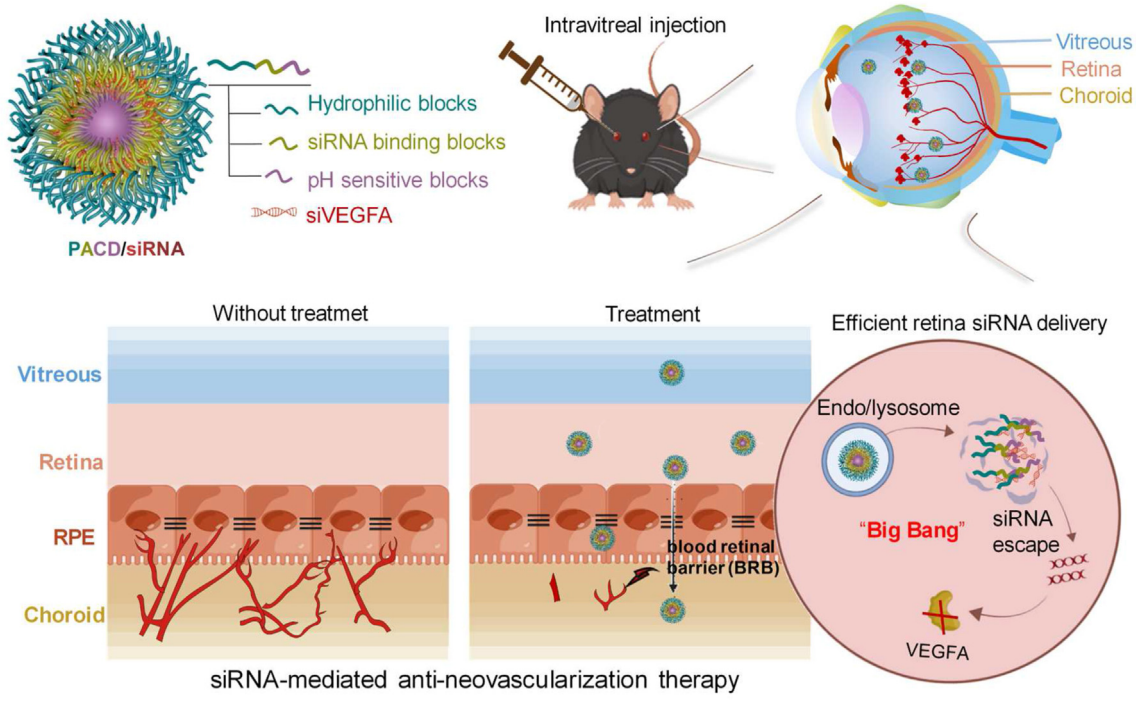

Figure 1 Schematic illustration of PACD polymeric micelle enabling efficient siRNA delivery in the retina and abrogating hypoxia-induced angiogenesis.

experiments and human resource use were approved by Wenzhou Medical University.

2.2. *Copolymer synthesis*

For the AMA-Boc synthesis, the 2-aminoethanol was first protected by di-*tert*-butyl dicarbonate. Following the reaction of methacryloyl chloride and *tert*-butyl *N*-(2-hydroxyethyl) carbamate, AMA was obtained. For the C7A-MA monomer synthesis, 0.15 mol C7A and 1.66 mol triethylamine (TEA) were dissolved in 150 mL tetrahydrofuran (THF) and stirred on ice. Then 0.168 mol methacryloyl chloride in 10 mL THF was dropwise added to the above mixture and the reaction was carried out overnight. Finally, hydroquinone was added to stop the reaction, and the crude C7A-MA product was obtained by vacuum distillation.

The preparation of DBA-AMA monomer was carried out using the previously reported modified method. Briefly, dissolve 0.8 mol 1-bromobutane and 0.4 mol ethanolamine in 800 mL CH_3CN, then add 1 mol Na_2CO_3 and stir all the liquid overnight at room temperature. Finally, the by-products and solvent were removed by dialysis and vacuum distillation, and the intermediated product 2-(dibutyl amino) ethanol was obtained. Then, 0.232 mol 2-(dibutyl amino) ethanol and 0.36 mol TEA were dissolved in 300 mL THF and stirred on ice. Drop 0.28 mol methacryloyl chloride in 10 mL THF into the mixture and stir overnight. Finally, hydroquinone was added to stop the reaction, and the DBA-AMA product was obtained by vacuum distillation.

The tri-block copolymer PACD was prepared by reversible addition-fragmentation chain transfer (RAFT) polymerization method. Specifically, 0.6 mmol PEG-CTAm (the micro-RAFT) was mixed with 30 mmol AMA monome in 10 mL Dimethylformamide (DMF), and the reaction was carried out with stirring for 24 h with AIBN as initiator. After the reaction, the solvent was removed by dialysis. The product PEG-b-PAMA was lyophilized and identified using ^{1}H NMR. The next two blocks were added to the chain. 3 mmol C7A-MA, 3 mmol DBA-MA and 0.06 mmol PEG-*b*-PAMA were mixed together in 6 mL DMF, and 10 mg AIBN was added into the mixture to initiate the reaction. The solvent and unreacted reagents were dialyzed after 24 h of stirring at room temperature. Lyophilized the final PEG-*b*-PAMA-*b*-P(C7A-r-DBA) product. All the monomers and block copolymers were characterized by ^{1}H NMR and GPC.

2.3. *PACD/siRNA polyplexes preparation and characterization*

The nanoprecipitation method was used to prepare PACD polymeric micelles. Specifically, the PACD powder was dissolved in 1 mL trifluoroethanol. Then, the PACD solution was added into phosphate buffer saline (PBS) ten times its volume and stirred at room temperature to evaporate the organic solvent. After the organic solvent was evaporated at room temperature overnight, the mixture was immediately dialyzed at room temperature for 24 h to ensure the complete removal of residual organic solvent. The prepared PACD nanomicelles were a clear, non-colorless solution. Before use, the nanomicelles were stored at 4 °C. To prepare the PACD/siRNA polyplex, mix the siRNA solution and PACD nanomicelles together and incubate at room temperature for 15 min. Transmission Electron Microscope (TEM) (HT7700, Hitachi, Tokyo, Japan) was used to examine the morphology and size of nanomicelles. Dynamic light scattering (DLS, Nano-ZS, Malvern, Worcestershire, UK) was applied to determine zeta potential and size distribution.

2.4. *siRNA release assay*

To investigate the release kinetics of PACD/Cy5-siRNA polyplexes, Cy5-labeled siRNA (Cy5-siRNA) was encapsulated into

PACD micelles. Subsequently, a dialysis process was performed at 37 °C using PBS (pH 7.4 and 5.5) to simulate the extracellular and acidic endosomal environments. At predetermined time points, three dialysis bags were taken out and the nanoparticle solution inside was aspirated, followed by adding methanol to fully release the siRNA. Cy5 fluorescence intensity was measured with a multimode microplate reader (excitation/emission, 540/570 nm) (Promega, Madison, WI, USA), and a standard curve correlating fluorescence and siRNA concentration was used to determine the amount of siRNA released from the polyplexes.

2.5. Gel retardation assay

The binding potential of PACD to siRNAs was evaluated using 2% agarose gel electrophoresis. To start, a series of PACD/siRNA polyplexes with varying weight ratios were prepared. Then, 0.5 μg siRNA from each sample was loaded into the agarose gel with a loading buffer and run for 15−20 min at 130 V. Finally, the agarose gel was photographed using a UV imaging system (Tanon, Shanghai, China).

2.6. pH-Sensitive test

The pH-sensitive properties of PACD and PACD/siRNA polyplexes were evaluated using the standard Nile Red encapsulation method. First, nanomicelles or polyplexes containing Nile Red were prepared by nanoprecipitation or incubation methods, respectively. Solutions with varying pH levels (ranging from 5.5 to 8.0) were then prepared. Next, 100 μL of PACD or PACD/siRNA polyplex solution was added into 1 mL PBS solutions with different pH levels. After a 2-h incubation at room temperature, the fluorescence intensity of Nile Red in each sample was measured using a multimode microplate reader (Promega).

2.7. In vitro gene silence potency

Real-time PCR was conducted to evaluate the gene silencing potency by assessing the relative levels of VEGFA mRNA. In brief, cells were inoculated at a density of 1×10^5/mL in 6-well plates and cultured in complete medium overnight. The cells were then transfected for 4 h with various PACD or Lipofectamine formulated siRNAs at 50 nmol/L. After 20 h, the transfection medium was replaced with complete medium and the cells were cultured again. Total RNA was extracted from the cells using the Trizol reagent, followed by reverse transcription into cDNA and PCR amplification. The mRNA levels of VEGFA were normalized to endogenous GAPDH mRNA levels. The Supporting Information Table S1 provides a list of the primers used for PCR. The efficacy of VEGFA protein expression associated with siRNA silencing was determined using Western blotting. Briefly, cells were transfected as described above and then lysed with RIPA lysis buffer (Beyotime, Shanghai, China). Total protein was quantified using a BCA kit (Lot#CW0014, CWBIO, Beijing, China). Equal amounts of protein were separated on a sodium dodecyl sulfate-polyacrylamide gel and transferred to a nitrocellulose membrane. The membranes were blocked for 1 h at room temperature with 5% bovine serum albumin (BSA) before being incubated with the primary antibody against VEGFA (ab214424, Abcam, Boston, MA, USA) or tubulin overnight at 4 °C. The membranes were then incubated with the Horseradish Peroxidase (HRP)-conjugated secondary antibody for 1 h. Finally, the membranes were imaged using a multi-imaging system (Tanon, Shanghai, China).

2.8. Cell cycle analysis

HUVEC cells were transfected with Lipo/siNC (non-sense control siRNA), Lipo/siVEGFA, and PACD/siVEGFA at concentrations of 50, 100, and 200 nmol/L, respectively. The control group ("Mock") consisted of untreated cells. After treatment, cells were washed with cold PBS buffer, harvested, and fixed. Propidium Iodide (PI) dye was added to the cell solution at a concentration of 1 μg/mL, followed by incubation for 30 min in the dark at 37 °C. The fluorescence at 488 nm was detected using flow cytometry (BD Biosciences, San Jose, CA, USA), and the DNA content of each sample was analyzed using FlowJo software.

2.9. Endocytosis mechanism

The ARPE-19 cells were pretreated with various endocytosis inhibitors, including chlorpromazine (to block clathrin-mediated endocytosis), amiloride (to inhibit macropinocytosis), genistein (to inhibit caveolae-dependent endocytosis), and methyl-β-cyclodextrin (M-β-CD) (to inhibit lipid raft-mediated endocytosis) for 30 min, before being treated with PACD/siRNA (Cy5-labeled) polyplexes for 4 h. To inhibit the energy-dependent pathway of PACD/siRNA, the cells were incubated at 4 °C for 30 min prior to treatment. The fluorescence intensity and cellular uptake rate were analyzed and quantified using flow cytometry (BD Biosciences). The uptake efficiency was calculated as the percentage of Cy5-positive cells in the total cell population.

2.10. Tube formation assay

HUVEC cells in passage 5 (P5) were seeded in 6 well plates at a cell density of 1×10^5/mL and cultured overnight in complete medium. The cells were then transfected with different groups of siRNAs for 6 h before being digested into a single cell. Meanwhile, the matrigel was applied to a precooled 96-well plate. After briefly cooling the liquid Matrigel and 96-well plate at −20 °C, 50 μL of Matrigel was quickly added to each well and incubated at 37 °C for 30 min to form a gel. The transfected cells were then seeded onto the surface of the gel at a density of 2×10^4 cells/100 μL and cultured for 12 h. Images of cell morphology were captured using a microscope system (Olympus X71, Nikon, Tokyo, Japan). Microvessel tubes with more than three junctions were analyzed for length and area using ImageJ software.

2.11. In vitro BRB model penetration experiment and transcytosis evaluation

To assess the ability of PACD/siRNA to cross the BRB *in vitro*, HUVEC cells were seeded in the top chamber of a 6-well Transwell plate insert containing a permeable membrane and cultured for one week. The insert was then placed onto a 6-well companion plate containing ARPE-19 cells in the bottom chamber. After continuing to culture for 24 h, PACD/Cy5-siRNA complexes with 50 and 150 nmol/L siRNA were respectively transfected into HUVEC cells. Following 4 h of transfection, the presence of Cy5 fluorescence in ARPE-19 cells was detected *via* flow cytometry (BD Biosciences).

For transcytosis evaluation, Firstly, the HUVEC and ARPE-19 cells were seeded on the coverslips (i), (ii), respectively (Supporting Information Fig. S7), and incubated for 24 h. The HUVEC cells on the coverslip (i) were first transfected with the PACD/Cy5-siRNA (50 nmol/L) for 8 h, followed by washing with

PBS three times. Secondly, the HUVEC cells on the coverslip (i) were co-incubated with ARPE-19 cells on the coverslip (ii) in fresh media for 8 h. At last, the cells were all collected and washed with PBS three times before analysis by FACS Calibur flow cytometer (BD Biosciences).

2.12. Intracellular distribution analysis

ARPE-19 cells were first transfected with various groups of siRNAs before being observed using confocal laser scanning microscopy (LSM700, Carl Zeiss, Jena, Germany). Cells were seeded in 20 mm dishes at a density of 2×10^5 cells per well and cultured overnight. The cells were then transfected with a 9/1 weight ratio of PACD/siRNA (Cy5 labeled) for 1, 3, 5, and 8 h, respectively. Following that, cells were stained for 20 min with Lysotracker Green and Hoecht 33342 and examined using laser confocal microscopy (Carl Zeiss). In the meantime, co-colocalization analysis between Cy5 and Lysotracker green was performed using Pearson's correlation coefficient, and the distance between red and green fluorescence was quantified using at least four images from different fields of view. In addition, chloroquine and bafilomycin A1 were used to investigate the endosomal disrupting and RNA silencing relationship[13–15]. Cells were firstly pretreated with 50 μmol/L chloroquine or 100 nmol/L bafilomycin A1 for 1 h. Following that, cells pre-treated with chloroquine or bafilomycin A1 were transfected for 4 h with either Lipo/siRNA or PACD/siRNA with chloroquine. Cell staining, mean fluorescence intensity quantification, and co-colocalization were all investigated. ARPE-19 cells were transfected as previously described in order to perform fluorescence-activated cell sorting (FACS). The cells were then washed with PBS buffer, digested with trypsin, washed twice more with PBS, and suspended in 0.5 mL PBS buffer. Following that, flow cytometry (BD Biosciences) was used to detect the intensity of the Cy5 fluorescence, and the data were analyzed using the Flowjo 7.6.1 software.

2.13. Mouse model of oxygen-induced retinopathy (OIR)

As previously reported[16], OIR was induced in C57BL/6J mice. Briefly, litters of postnatal Day 7 (P7) mice were placed in an incubator with 75% oxygen atmosphere for 5 days (P12) with their feeding mothers after birth. The mice were then returned to normal room air. All OIR-induced mice were randomly assigned to one of four groups (control, ranibizumab, PACD/siNC (2 μg siRNA), and PACD/siVEGFA (2 μg siRNA) and intravitreally injected with 0.5 μL of various drugs. All mice were sacrificed at P17, and the eyeballs were enucleated for further retina analysis.

2.14. Intraocular distribution

For the intraocular distribution and metabolic study, C57BL/6J male mice aged 6 weeks were used. Mice were first deeply anesthetized with intraperitoneal injections of chloral hydras (240 mg/kg) and xylazine (14.4 mg/kg), followed by topical anesthetic proparacaine hydrochloride eye drops (0.5% wt/vol). Mice were randomly divided into four groups and intravitreally injected with sterile PBS, siNC, PACD/siNC, PACD/siVEGFA at a dosage of 2 μg siRNA, all of which were labeled with Cy5. Four mice from each group were sacrificed with excessive isoflurane exposure at 3, 6, 12, 24 h, Days 3, and 7 after injection. The mice's eyes were embedded with optimal cutting temperature compound (OCT), and then frozen sections of the eyes were examined under a confocal laser scanning microscope (Carl Zeiss).

2.15. Imaging and immunofluorescent staining of retinal tissue

OIR mice were first given a variety of formulations. Mice were sacrificed at P17, and their eyeballs were immediately enucleated and fixed for 1 h. Following that, the vitreous body was completely removed and the retinas were washed three times in PBS. To make retina flat mounts, the retinas were cut into the shape of a four-leaf clover. For detecting neovascular vessels, the retinas were stained overnight with Isolectin GS-IB4 dye (Molecular Probes). For detecting vascular leakage, the retinas were first blocked with 5% BSA at room temperature, then incubated with mouse TER-119 antibody (MAB1125, R&D system) overnight at 4 °C, followed by a secondary antibody incubation for 2 h at room temperature. Observation of retinas was conducted under a Confocal laser scanning microscope (Carl Zeiss). The pathological neovascularization was outlined, and the neovascular area and red blood cell leakage area were measured using Adobe Photoshop software (Photoshop CC). The percentages of neovasculature and RBC leakage were calculated as the ratio of neovascular or RBC leakage areas to the total retina area. The P17 OIR mice were deeply anesthetized for fundus angiography, as previously described. A drop of 1% tropicamide was used to dilate their pupils. The mice were then injected intraperitoneally with 0.01 mL of 25% sodium fluorescein (Akorn Inc, Lake Forest, IL, USA) per 5 g body weight. Images of fundus angiography were taken under UV light using the Micron IV retinal imaging system 2−5 min after fluorescein injection. For H&E staining, mouse eyeballs were first fixed with eye fixation fluid (methanol: chloroform: glacial acetic acid = 6:3:1, *v*/*v*/*v*) overnight, then dehydrated in alcohol and embedded in paraffin. The whole eye sections were stained with hematoxylin and eosin. The separated retinas were also used to assess the level of VEGFA mRNA and protein expression. To extract total RNA or protein, fresh mice retina was first crushed using an ultrasonic crushing instrument in either Trizol reagent or lysis buffer. Following that, real-time PCR and Western Blotting were used to detect the mRNA and protein content in tissues.

2.16. H&E staining of major organs

PBS, PACD/siNC, ranibizumab, and PACD/siVEGFA were given to normal C57BL/6J mice at random. All mice received a 2 μg dose of siRNA intravitreally. Mice were sacrificed 24 h after injection, and their major organs were fixed and stained with H&E. Similarly, PBS, naked siNC, PACD/siNC, and PACD/siVEGFA were also given to normal C57BL/6J mice at random. Mice were sacrificed 24 h and Day 7 after injection, and their eyeballs and brains were fixed and stained with H&E.

2.17. Data analysis

All data are presented as mean ± SD or mean ± SEM in this study. Statistical analysis was conducted by using GraphPad Prism 9.0 software. Student's *t*-test and one-way ANOVA tests were used to determine whether there was a significant difference at $P < 0.05$.

2.18. Ethics statement

The animal experiments complied with the Association for Research in Vision and Ophthalmology (ARVO) Statement Regarding the Use of Animals in Ophthalmic and Vision

Research. All experimental procedures were executed according to the protocols approved by the Animal Care and Ethics Committee at Wenzhou Medical University. The approval number is "wydw2022-0069".

3. Results and discussion

3.1. PACD synthesis and characterization

In order to synthesize a typical A-B-C tri-block copolymer, we selected poly (aminoethyl methacrylate) (PAMA), a highly efficient gene delivery cationic polymer, as the siRNA binding segment. The pH-responsive segments 2-(hexamethylenediamine) ethyl methacrylate (C7A-MA) and 2-(dibutyl amino) ethyl methacrylate (DBA-MA) were used as hydrophobic segments, and PEG as hydrophilic segments. Increasing evidence shows that pK_a values around 6.0 have important effects on the RNA delivery efficiency of ionizable lipids[17,18]. Considering that a similar rule may apply to polymers, we optimized the number of C7A-MA and DBA-MA monomers with pK_a values of 6.8 and 5.2, respectively, to obtain an appropriate pH-sensitive copolymer. Finally, the copolymer PACD was optimized and synthesized. The synthesis route of the tri-block copolymer is shown in Supporting Information Fig. S1. Briefly, three monomers were synthesized first. Subsequently, a tri-block copolymer was synthesized according to the reversible addition-fragmentation chain transfer (RAFT) polymerization method by adding various monomers sequentially. The ^{1}H NMR results shown in Supporting Information Figs. S2 proved that the monomers and PACD were successfully synthesized.

In addition, we evaluated the siRNA binding ability of PACD. Since PACD is amphiphilic, it can easily assemble into polymeric nanomicelles with a hydrophobic core and hydrophilic shell structure by using the solvent evaporation method. Through electrostatic adsorption interactions, siRNA binds to PEG-PAMA segments to form the PACD/siRNA polyplex (Fig. 2A).

The ability of PACD and PACD/siRNA polyplexes to release encapsulated molecules in endosomal/lysosomal acidic pH environments was evaluated using the classic Nile red encapsulation method. Hydrophobic Nile red was encapsulated into the hydrophobic core of PACD micelles as a model drug for pH-sensitivity evaluation. The release of Nile red from the micellar environment to various acidic environments was monitored by detecting the fluorescence of the dye. As shown in Fig. 2B and C, the fluorescence intensity of Nile red showed very limited differences near the physiological pH (pH 6.5−8.0), indicating that the micelles were stable within the physiological pH range. As the pH value

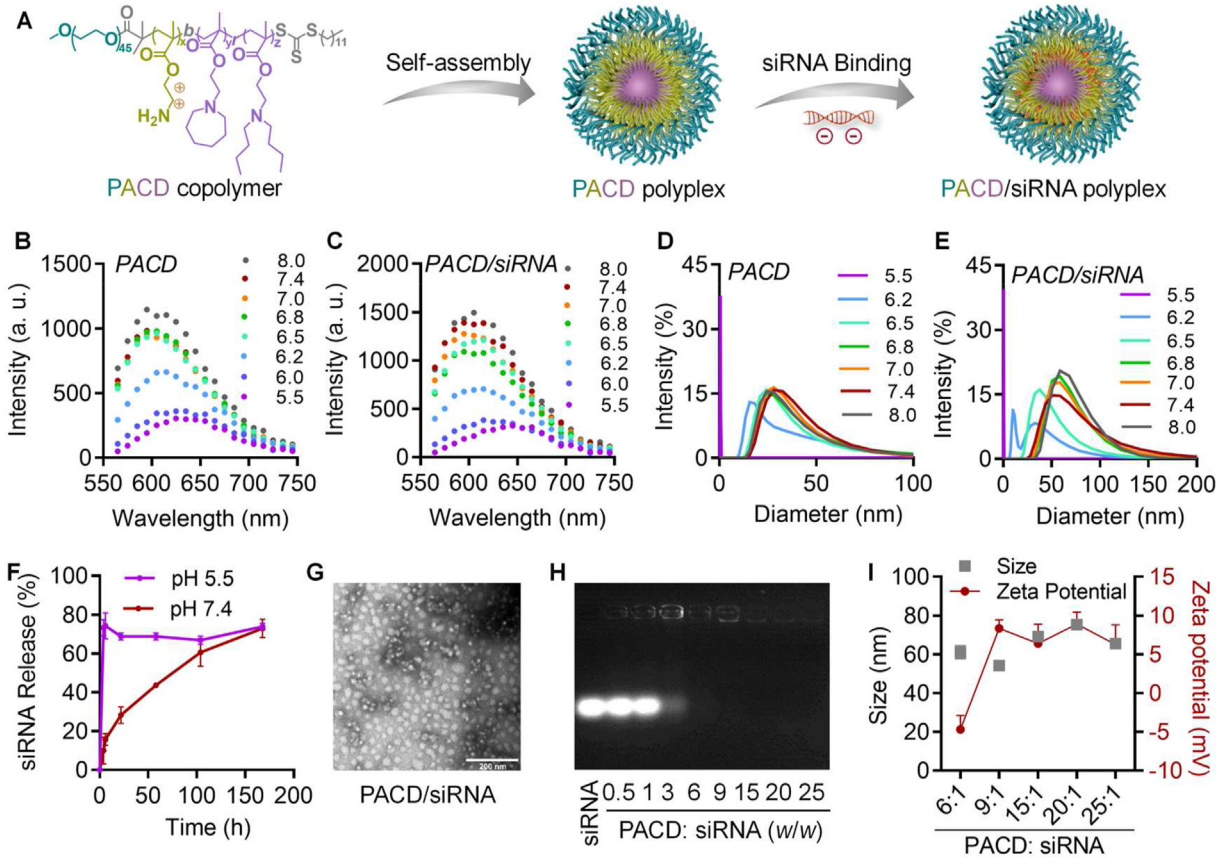

Figure 2 Characterization of PACD/siRNA polyplex. (A) Schematic illustration of PACD and PACD/siRNA polyplex preparation. The assembly and disassembly characteristics of PACD (B) and PACD/siRNA (C) polyplexes with varying pH values were evaluated by Nile red fluorescence probe method. (D, E) The associated size changes were evaluated by the DLS equipment (Malvern). (F) The release profile of siRNA at pH 7.4 and 5.5. Data are expressed as mean ± SD; $n = 3$. (G) TEM image of the polyplexes/siRNA (Scale bar: 200 nm). (H) Agarose gel retardation assay was used for the optimization of the rational compact weight ratio of PACD: siRNA. (I) Size distribution and zeta potential of PACD/siRNA polyplexes at various weight ratios. Data are expressed as mean ± SD; $n = 3$.

dropped, the fluorescence decreased gradually. At a pH of 6.2, the fluorescence intensity of Nile red decreased significantly, suggesting that Nile red was released from the hydrophobic core of micelles under weakly acidic conditions. PACD and PACD/siRNA polyplexes showed similar profiles. We also measured the size of polyplexes under various pH conditions. PACD polyplexes have a constant size of around 30 nm in a near-neutral environment. However, as the pH decreases, the size keeps reducing. When pH is below 5.5, no size distribution can be detected, suggesting that the micelles are completely destroyed. PACD/siRNA polyplexes showed the same tendency (Fig. 2D and E). Consistently, PACD and PACD/siRNA polyplexes exhibit lower Polydispersity Index (PDI) values at near-neutral conditions (Supporting Information Fig. S3). It is well known that early endosomes exist in an acidic environment with a pH of 6.5−5.5. The robust changes of PACD particle size under different pH conditions indicate that PACD is relatively stable and complete at neutral pH, but it will trigger hydrolysis and release loaded siRNAs when confronted with a similar acidic environment of endosomes. The siRNA release data also showed that PACD micelles exhibited rapid and robust release at pH 5.5, indicating that the intracellular acidic environment in the cytoplasm may significantly facilitate siRNA release inside cells. In contrast, at pH 7.4, siRNA was slowly released and had sustained release for up to Day 7, providing further evidence of strong electrostatic interaction between the polyplexes and siRNA in the physiological extracellular environment (Fig. 2F).

Further, we investigated the siRNA loading capacity of PACD. Various polyplexes with different PACD to siRNA weight ratios

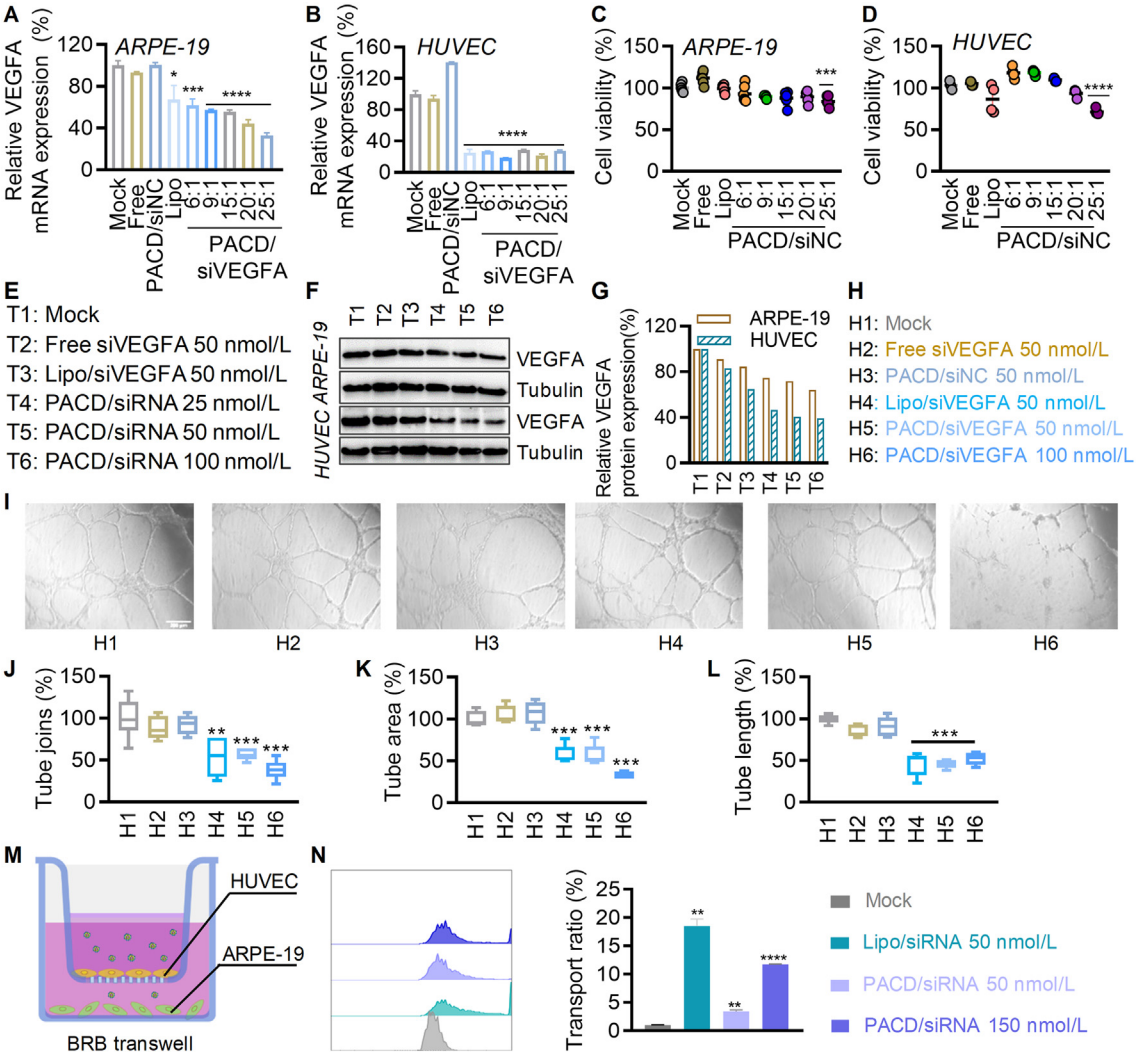

Figure 3 *In vitro* gene silencing and anti-neovascularization effects of PACD/siRNA. (A) The VEGFA mRNA expression of ARPE-19 (A) and HUVEC cells (B) with various polymers to RNA weight ratios. (A and B, mean ± SD; $n = 3$) The cell viability of ARPE-19 (C) and HUVEC cells (D) in various polymers to siRNA weight ratios. (C, mean ± SD; $n = 6$) (D, mean ± SD; $n = 4$) (E) The information of the groups in Fig. 3F and G. (F)Western blotting of VEGFA proteins in cell lysates and quantification of the blotting bands (G). (H) Group information of Fig. 3I−L. The tube formation of HUVEC cells on Matrigel was evaluated in observation (I) and tube joints (J), tube area (K), and tube length (L), the quantification was measured using the ImageJ software. Scale bar: 200 μm. (M) Transwell co-culture model. The co-cultured cells on the top and bottom of the Transwell chamber were not in direct contact. (N) Flow cytometry detection of Cy5-siRNA fluorescence and transport ratio analysis of PACD/Cy5-siRNA in the lower layer of ARPE-19 cells at final siRNA concentrations of 50 nmol/L and 150 nmol/L (N, mean ± SD; $n = 3$). Data in J−L are represented as mean ± SD ($n = 7$). $^{*}P < 0.05$, $^{**}P < 0.01$, $^{***}P < 0.001$, $^{****}P < 0.0001$.

were prepared and evaluated using the gel retardation assay. As shown in Fig. 2H, siRNA could be fully loaded when the ratio of PACD to siRNA was above *6:1*. The resulting polyplexes were all spherical in shape, with a size of about 20−50 nmol/L (Fig. 2G, Supporting Information Fig. S4). The polyplexes formed by different ratios of PACD and siRNA had limited particle size changes and a slightly positive charge (Fig. 2I).

3.2. In vitro gene silencing and neovascularization regulation of PACD/siRNA polyplexes

Neovascularization mainly depends on endothelial cell proliferation, migration and differentiation to form a vascular network. The VEGF family is currently the main target of anti-angiogenesis therapy[19]. Abolishing VEGFA, which is the most abundant member among the VEGF family, is an important therapeutic approach to treat neovascular ocular diseases. Therefore, the siRNA targeting both human and mouse *Vegfa* genes was chosen. To enhance stability and reduce the off-target effect, the full sequence of siRNA was modified in a site-specific manner, with ribose modification at the 2′-OH position by 2′-*O*-methyl (2′-OME) or 2′-deoxy-2′-fluoro (2′-F) substitution and phosphonate linkage modification with phosphorothioate (PS). The chemical modification did not affect siRNA efficiency at all (Supporting Information Fig. S5).

Next, we evaluated the gene silencing efficiency of PACD/siRNA polyplexes on human retinal cells (ARPE-19) and human primary umbilical cord blood vascular endothelial cells (HUVEC). As shown in Fig. 3A, the VEGFA mRNA expression in ARPE-19 cells decreased as the weight ratio of PACD to siRNA increased. In HUVEC cells, gene silencing activity was even

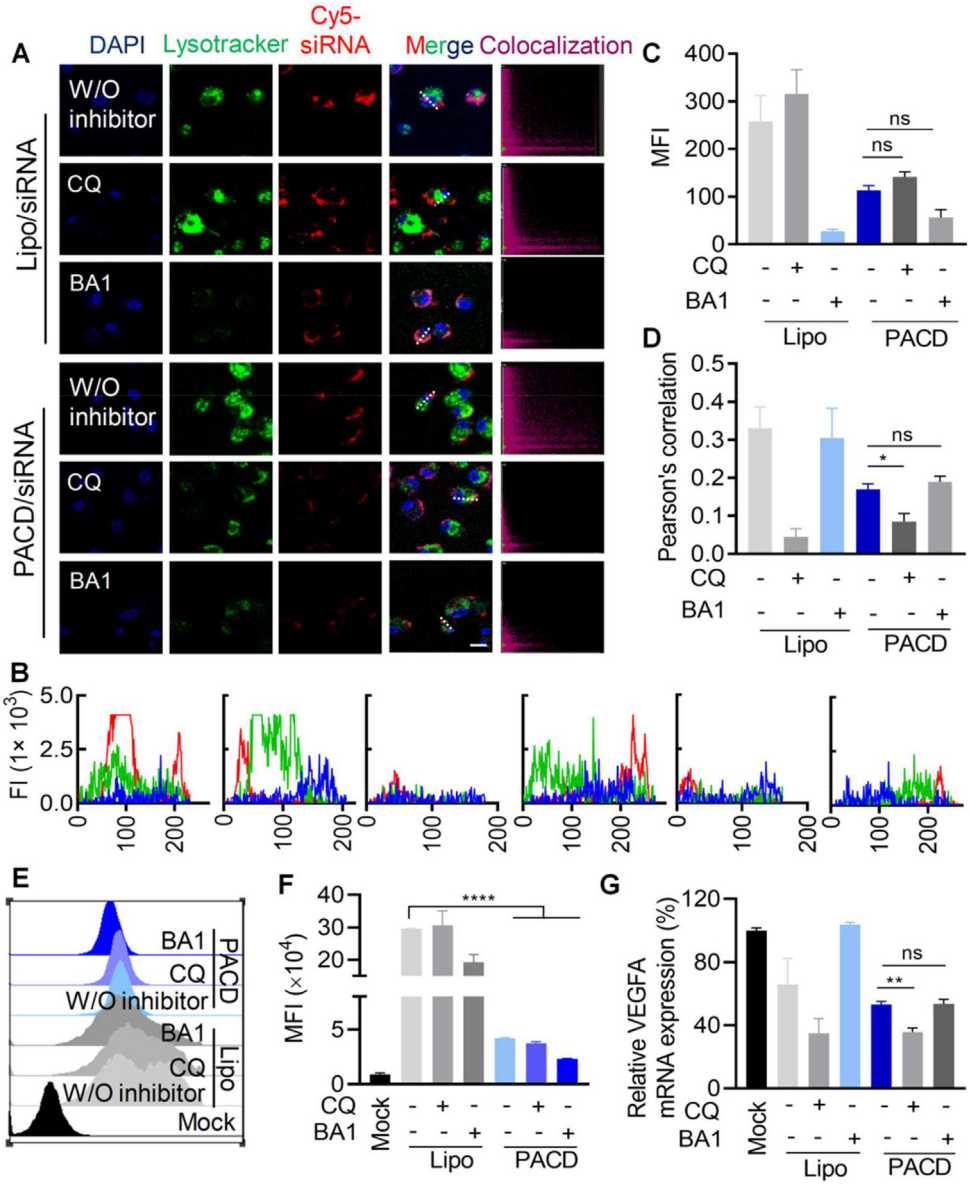

Figure 4 Intracellular siRNA distribution and PACD-assisted siRNA endosome escape capacity. (A) Comparison of endosome escape capacity of Lipo/siRNA and PACD/siRNA polyplexes with or without the addition of CQ or BA1. The scale bar was 15 μm. (B) The distance of siRNA and lysotracker in (A). (C, D) MFI and colocalization analysis of (A) and (B). (E) and (F) Flow cytometry analysis of PACD/siRNA polyplexes under various conditions. (G) The relative VEGFA mRNA expression of each group was quantified by real time-PCR. Data in C, D, F, and G are represented as mean ± SD ($n = 3$). *$P < 0.05$, **$P < 0.01$, ****$P < 0.0001$, ns, no significant difference.

stronger than in ARPE-19 cells. When the siRNA transfection concentration was 50 nmol/L and the PACD/siRNA ratio was 9/1, only 18% of VEGFA mRNA expression remained (Fig. 3B). Meanwhile, Lipofectamine2000 (Lipo) was comparable to a 6/1 ratio of PACD/siRNA in gene silencing efficiency but was not competitive with a higher PACD/siRNA ratio. Neither free siRNA nor PACD/siNC (scrambled sequence siRNA) showed any gene silencing. The cell viability results showed that when the ratio of PACD to siRNA was less than 20/1, cytotoxicity to the two cells was negligible (Fig. 3C and D). By balancing gene silencing efficiency and cell viability, we screened a 9/1 ratio of PACD/siRNA for subsequent evaluation. As can be seen from Fig. 3E–G, PACD/siRNA reduces VEGFA protein levels in a dose-dependent manner. Even at a low siRNA transfection concentration of 25 nmol/L, the target protein knockdown efficiency of PACD/siRNA was better than that of Lipo/siRNA at twice the transfection concentration.

Subsequently, the effect of PACD/siVEGFA transfection on the cell cycle was evaluated. As shown in Supporting Information Fig. S6, the G2/M phase was increased in the PACD/siVEGFA groups transfected with 100 and 200 nmol/L siRNA, while no significant differences were observed between the Lipo/siVEGFA group and the PACD/siVEGFA group containing 50 nmol/L siRNA when compared to the Lipo/siNC group. To further evaluate the gene silencing effect on HUVEC angiogenesis, the *in vitro* tube formation assay was performed. Neither free siVEGFA nor PACD/siNC showed any inhibitory effect on tube formation from cell plate photos and quantitative results (Fig. 3H–L). Both Lipo and PACD showed significant inhibition on tube joint numbers, tube areas and length at 50 nmol/L. With the increase of transfection concentration, the PACD group showed better tube inhibition efficiency. As is well known, the BRB is a natural biological barrier within the eye, and drugs must penetrate the BRB to achieve effective retinal therapy. *In vitro*, transwell BRB model and transcytosis experiments were performed to demonstrate the BRB-penetrating ability of PACD/siRNA. As shown in Fig. 3M and N, Cy5-siRNA fluorescence signals were detected in the lower layer ARPE-19 cells, indicating that PACD/Cy5-siRNA successfully penetrated the upper layer of endothelial cells. The transcytosis experiment further demonstrated that PACD/Cy5-siRNA may penetrate the BRB and reach retinal cells by transcytosis uptake (Supporting Information Fig. S7).

In order to clarify the mechanism of endocytosis of PACD/siRNA polyplexes, we performed the endocytosis inhibition experiment. Flow cytometry analysis showed that Amiloride, chlorpromazine, genistein, and M-β-CD all blocked the polyplexes' cellular internalization, but were less effective than low temperature (Supporting Information Fig. S8), suggesting that PACD/siRNA polyplexes could transport into cells through multiple endocytosis pathways.

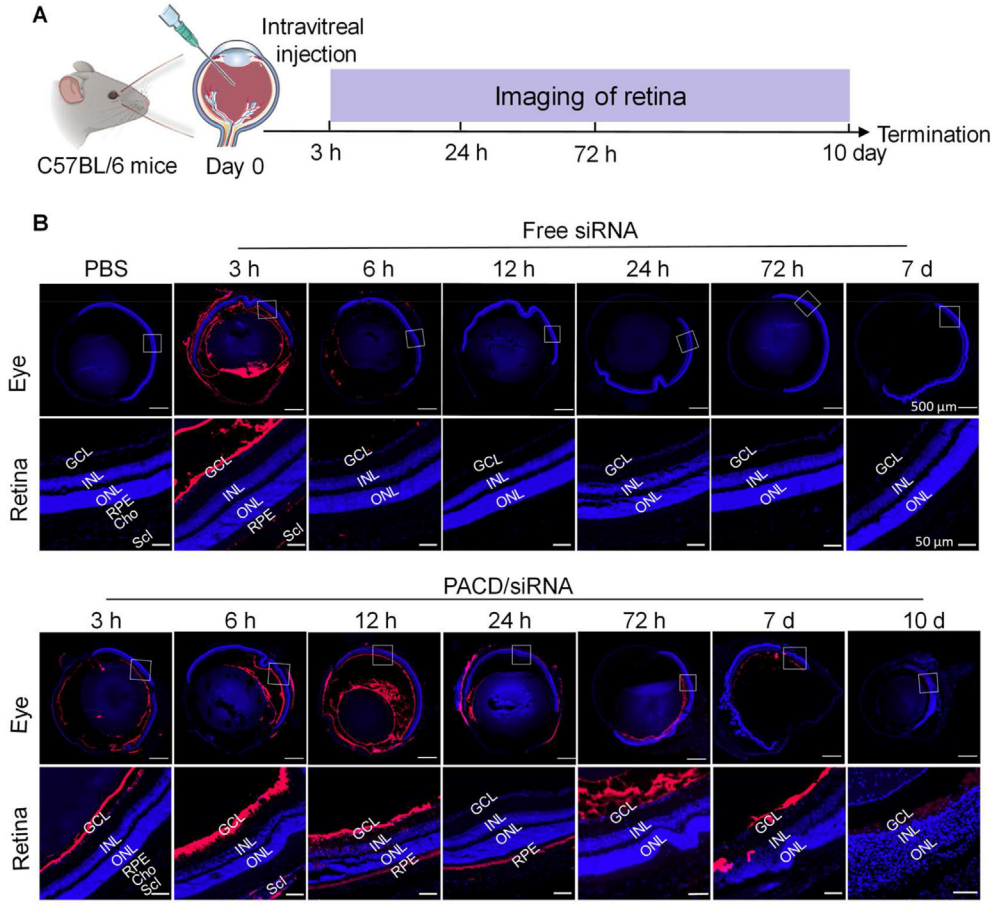

Figure 5 Intraocular distribution of PACD/siRNA. (A) Schematic illustration of eye imaging process in mice. (B) Distribution of PACD/siRNA (Cy5-siRNA) in mouse retina at 3, 6, 12, 24, 72 h and Day 7, 10 after single intravitreal injection. GCL, INL, ONL, Cho and Scl represent the ganglion cell layer, inner nuclear layer, outer nuclear layer, Choroid layer and Sclera, respectively. (Eye, scale bar = 500 μm; Retina, scale bar = 50 μm).

3.3. The pH-responsive cytosolic release mechanisms of PACD/siRNA

To elucidate the underlying mechanism of PACD/siRNA-mediated efficient gene silencing, we carefully studied the internalization and intracellular trafficking of PACD/siRNA polyplexes in ARPE-19 cells at different transfection time points. We found that the fluorescence of siRNA increased with the extension of siRNA transfection time, indicating that the uptake of siRNAs was time-dependent (Supporting Information Fig. S9A). The mean fluorescence intensity also tells the same tendency (Fig. S9C). Meanwhile, the co-localization of lysotracker green and Cy5-siRNA red fluorescence signals in ARPE-19 cells was analyzed. Initially, green and red fluorescence were fairly colocalized together, however, with increased cell uptake at 5−8 h, a low colocalization tendency emerge (Fig. S9B). Pearson's correlation quantization may more directly reflect this tendency, with a smaller correlation coefficient indicating that more siRNAs escape from endosomes and thus are distributed in the cytoplasm (Fig. S9D).

In order to reveal whether PACD-mediated gene silencing is more dependent on cellular uptake or endosome escape, we used the endosome disrupting agent chloroquine (CQ, an endosome escape promoter) and bafilomycin A1 (BA1, an endosome escape inhibitor). The specific behaviors of Lipo and PACD during siRNA delivery were compared as shown in Fig. 4A, B, E, and F, the initial cellular uptake of PACD/siRNA was much weaker than that of the Lipo/siRNA group. CQ treatment did not affect cell uptake of siRNA in Lipo and PACD groups, but significantly reduced the Pearson's correlation coefficient of siRNA and lysotracker, while BA1 treatment decreased cell uptake of siRNA in both groups, but the Pearson's correlation coefficient remained unchanged (Fig. 4C and D). In addition, we examined the relative mRNA expression between Lipo and PACD-formulated siRNAs. The gene silencing efficiency of PACD/siVEGFA without CQ or BA1 treatment was similar to that of the Lipo/siVEGFA group. After CQ treatment, gene silencing efficiency was improved in both groups (Fig. 4G), and the addition of BA1 did not affect mRNA expression level. These results clearly indicate that endosome escape is positively correlated with gene silencing efficiency. Considering that the endocytosis of Lipo was approximately 7 times that of PACD (Fig. 4E and F), but the siRNA silencing efficiency of PACD is comparable to that of Lipo, we believe that PACD has much better endosome escape efficiency than Lipo, which strongly emphasizes the large contribution of endosome escape to gene silencing. It is reported that, block copolymers with pH-responsive disassembly values (pH_{dis}) similar to the intracellular endosomal pH response to the endosome environment and disassemble[10]. As aforementioned, PACD was formed from three-block copolymers with a pH-sensitive core and hydrophilic shell. It can quickly disassemble at pH 6.2 and below. Thus, our PACD example provides further evidence that endosomal escape should be of greater concern than cellular uptake in the design of siRNA polymer delivery systems.

3.4. Intraocular distribution of PACD/siRNA

Although we have shown that PACDs exhibit excellent siRNA delivery in cell lines, achieving successful *in vivo* siRNA transfection in vascular retinas and choroids is a prominent challenge. To test whether PACD can transfer siRNA into mouse vascular retinal tissue, we intravitreally injected the PACD/siRNA into mouse eyes and evaluated the distribution and intraocular metabolism of siRNAs (Fig. 5A). As shown in Fig. 5B, 12 h after a single intravitreal injection, Cy5-siRNA was distributed throughout the retinal layers, including ganglion cell layer, inner nuclear layer, outer nuclear layer and RPE layer, indicating that PACD/siRNA can penetrate the inner barrier of the blood-retina barrier. Even after Day 10 post-injection, fluorescence signals were still detected in the ganglion cell layer, suggesting that the chemical modification and encapsulation of siRNA by PACD conferred long-term stability and persistence in the retinal tissues. In contrast, free Cy5-siRNA was rapidly eliminated in the eye 6 h after injection, with only weak fluorescence.

Typically, the intraocular clearance mechanism has a very adverse effect on the activity of intravitreal injection drugs[7,20]. These clearance mechanisms include the BRB, vitreous body and multilayers of retinal cells. Drug delivery to the posterior segment of the eye is a very challenging issue due to the BRB. The retinal barrier includes the inner barrier and the outer barrier, in which the inner barrier is retinal vascular endothelial cells and their tight junctions, while the outer barrier is the pigmented cuboidal epithelial cells in the outmost layer of the retina, forming the excellent barrier function of RPE[21]. These two parts play a crucial role in limiting the diffusion of drugs through the vitreous body and bloodstream into the eye.

In addition to BRB, the vitreous body also plays a very important role in drug adsorption. The vitreous body consists of more than 98% water, with collagen fibrils and hyaluronans forming an extensive and fine network structure. The pore size of the central vitreous mesh is between 500 and 1000 nmol/L[22]. It has been reported that the size, charge and surface coating of the delivery system have a great influence on its diffusion in the vitreous body[20]. For example, the commonly used PEI/DNA nanoparticles tend to aggregate in the vitreous body due to their high positive charge. In contrast, the dense PEG block polymer/DNA complex, with a near-neutral potential and a size of about 60 nmol/L, exhibits rapid diffusion in the vitreous body. PEG-coated dense, negatively charged, 100−750 nmol/L diameter polystyrene beads diffuse very rapidly in the vitreous body. For PACD/siRNA, it appears that the PEG hydrophilic shell and small size allow it to spread rapidly through the vitreous body to reach the retina within 6 h[20]. Considering the poor ability of negatively charged macromolecules such as siRNAs to penetrate cell membranes, the slightly positive charge of PACDs enables them to efficiently penetrate of BRB without affecting their diffusion ability, thus delivering siRNAs to retinal/choroid cells and maintaining them for a longer time.

3.5. Silencing VEGFA abrogated hypoxia-induced angiogenesis

Encouraged by the excellent *in vivo* distribution of PACD/siRNA polyplexes, we further explored whether PACD/siRNA can achieve the therapeutic effect of anti-retinal angiogenesis. As a result, at postnatal Day 12 (P12), we injected PACD/siVEGFA polyplexes intravitreally into the eyes of mice with the OIR model. The P7 mice pups together with their nursing mothers were subjected to a hyperoxia (75%) atmosphere for 5 days. During this period, retinal vessel growth is greatly inhibited and obvious vessel loss occurs. At P12, mice pups were returned to normal room air. The retinal hypoxia and avascular induce both normal vascular regeneration and retinal neovascularization, which reach the peak at P17 (Fig. 6A). As shown in Fig. 6B and C, on P17, the whole-mount retina staining indicated that the neovascularization

rate of the mice injected with PACD/siVEGFA was significantly reduced, suggesting that the silencing of VEGFA mRNA with PACD/siVEGFA could inhibit retinal neovascular. The clinical drug ranibizumab showed a comparable anti-neovascularization effect to PACD/siVEGFA polyplexes. Results of mRNA and protein expression levels of target genes showed that only the PACD/siVEGFA group had significantly decreased mRNA and protein expression (Fig. 6E–G). In addition, H&E staining of whole eye sections showed decreased retinal vascular lumen treated with PACD/siVEGFA. More importantly, no obvious inflammatory cell infiltration was detected (Fig. 6D).

One of the main consequences of abnormal neovascularization is possible leakage of blood cells, which can lead to blindness. Hence, we injected fluorescein intraperitoneally into P17 OIR mice and performed fluorescein angiography (FA) to monitor vascular leakage. As shown in Fig. 6H, both the ranibizumab and PACD/siVEGFA polyplex groups showed less fluorescein leakage than the control groups. Subsequently, the flat-mount retinas were stained with TER 119 (green) and IB4 (red) to label the red blood cell (RBC) and blood vessels. As shown in Fig. 6I and J, consistent with the FA images, retinal vascular leakage was reduced in both the ranibizumab group and PACD/siVEGFA

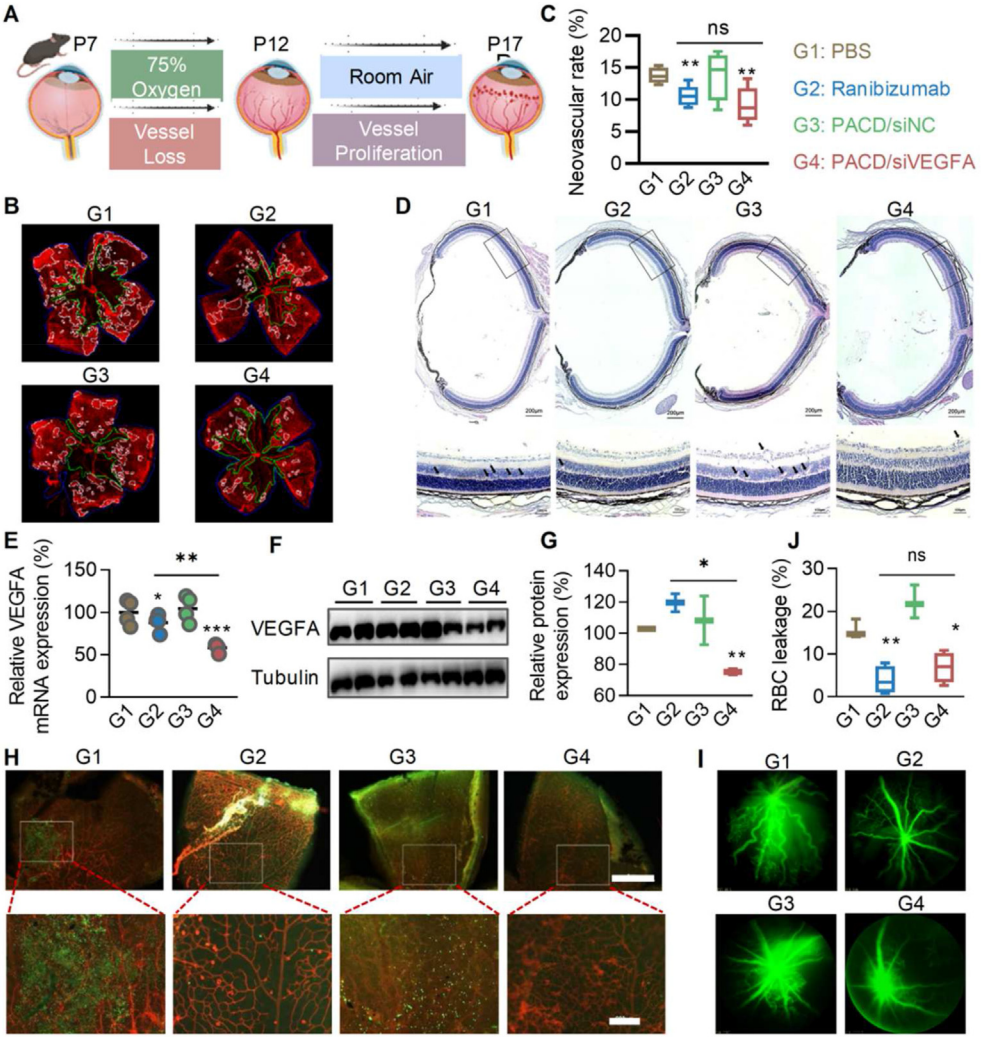

Figure 6 Anti-neovascularization of PACD/siRNA in an OIR mouse model. (A) Establishment of OIR mouse model and treatment schedule. P7 and P12 represent postnatal Days 7 and 12 for mice. (B) Whole-mount retina staining from sacrificed mice. All the retinas were stained with GS-IB4 (red). The blue, green and white lines represent the edge of the retina, non-perfusion area, and pathological neovascularization area. (C) The rate of retinal neovascularization in different treatment groups, as measured by the ratio of pathological neovascularization area to total retina area. (D) H&E staining of the whole eye section. Below is a zoomed-in view of the box area above. The scales are 200 μm (top) and 100 μm (bottom). The black arrow indicates the vascular lumen. (E) The relative VEGFA mRNA expression in the P17 mouse retina was evaluated by real-time PCR. (F, G) Western blotting images and quantification of VEGFA protein expression in each group. The blotting bands were quantified by Image J software. (H) Fundus fluorescein angiography of P17 mice. (I) Vascular leakage and staining of the retina flatmounts. The red blood cells were labeled with TER119 (green) antibody and the neovessels were labeled with isolectin GS-IB4 (red) antibody. The scale is 1 mm (top) and 200 μm (bottom). (J) Quantified statistical results of the percentage of RBC leakage in each group. The RBC leakage percentage was calculated by the ratio of the RBC area to the total retina area. One-way ANOVA was used to evaluate the statistical significance. Data in C, E, G and J are represented as mean ± SD ($n = 4$). *$P < 0.05$, **$P < 0.01$, ***$P < 0.001$. ns, not significant.

group, and there was no difference between them. Taken together, these results provide a solid foundation for PACD/siRNA gene silencing therapy for retinal neovascularization diseases.

Both ranibizumab and siVEGFA, two different forms of anti-VEGF drugs, have exhibited anti-retinal angiogenesis effects. Our findings reveal that siVEGFA can rapidly penetrate the BRB following intravitreal injection and remain in the retina for more than 10 days thanks to precise sequence design, chemical modification, and efficient PACD delivery systems (Fig. 5B). In comparison to antibodies, which have to be frequently supplied and injected, siRNA may be more convenient for patients. Furthermore, siRNA targeting mRNA is an information therapeutic that can theoretically be tailored to any gene and is reasonably easy to manufacture and produce in huge quantities. As a new generation of biotechnology therapeutics, siRNA has a very broad applicability possibility in ophthalmology.

3.6. *Safety evaluation*

To evaluate the *in vivo* safety of PACD, a hemolysis test and H&E staining were conducted. As shown in Fig. 7A and B, PACD/siRNA does not cause hemolysis under physiological pH conditions, but when pH is adjusted to 5.5, hemolysis occurs immediately in PACD/siRNA, which is similar to the positive lysis buffer (PLB). The

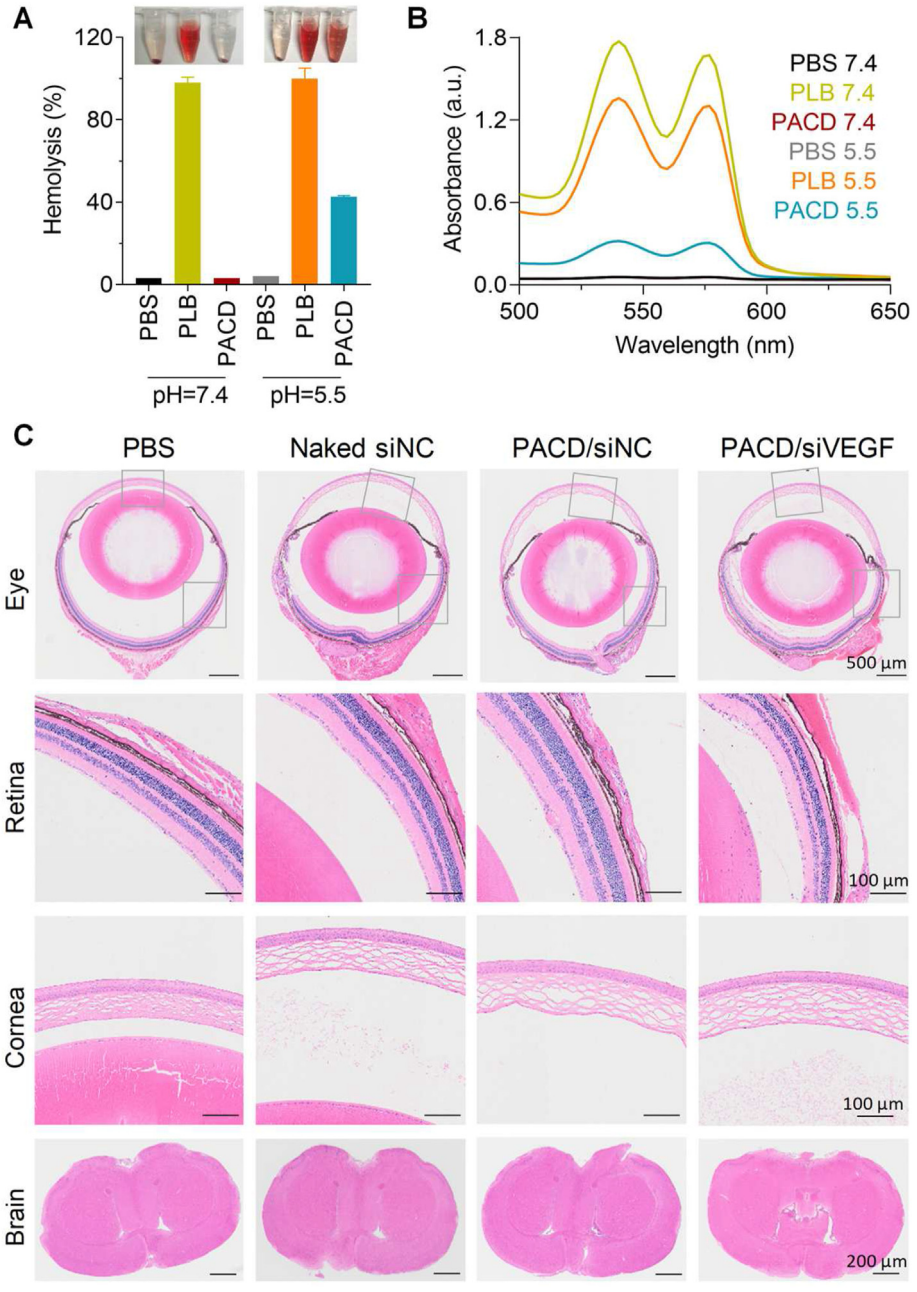

Figure 7 Safety evaluation of PACD/siRNA. (A) The blood compatibility of PACD/siRNA was measured by hemolysis assay. PBS and positive cell lysis buffer (PLB) were used as negative and positive controls, respectively. (B) Absorbance results of (A). (C) H&E staining of mouse eyeballs and brains after 24 h of intravitreal injection. Data in A are represented as mean ± SD ($n = 3$).

absorbance of all samples also revealed a consistent hemolysis tendency. These results reflect that PACD is compatible with blood cells in physiological environments, but leads to the destruction of cell membrane structures such as endosome membranes in an acidic environment. Meanwhile, we investigated the short-term (24 h) and long-term (Day 7) effects of intraocular siRNA injection on the eye, brain and major organs. H&E staining of sections showed no difference between PACD/siRNA groups and PBS buffer and did not cause any pathological changes in tissues and organs (Fig. 7C, Supporting Information Figs. S10 and S11).

It is worth noting that each polymer delivery strategy has distinct advantages, and the selection must be made based on the administration route and needed residence time. Although PACD is not biodegradable, its high stability can shield siRNA from chemical and enzymatic degradation, which is crucial for nucleic acid delivery. Furthermore, the nanosized PACD micelles can be endocytosed and remain in the retina tissue for up to 10 days (Fig. 5B). This may be due to the highly efficient transcytosis uptake and BRB penetration of PACD/siRNA polyplexes (Fig. 3M and N, and Fig. S7), as well as the multiple cellular endocytosis pathways. These characteristics provide the possibility to reduce the frequency of intravitreal administration and have a good application prospect of ophthalmic drugs.

Throughout the history of siRNA drug development, Bevasiranib targeting VEGFA and AGN211745 targeting VEGFR1 are two early siRNA therapeutics developed for AMD treatment[23]. In 2009, a study found that siRNA length of 21 nucleotides or longer suppressed CNV in mice by activating the TLR3 immune pathway, regardless of the siRNA sequence, a finding that dealt a fatal blow to siRNA drugs[24]. To overcome this deficiency of siRNA, various chemical modifications have been developed, including modifications on the phosphate backbone, ribose, or base. In our study, the full sequence of siRNA was modified with 2′-OME, 2′-F and phosphorothioate substitution. These modifications ensure an enhanced siRNA affinity to its target mRNA and a reduction *in vivo* immunogenicity without affecting its activity (Supporting Information Fig. S3). In addition to chemical modification, delivery systems also play an important role in maximizing the potency of siRNA and reducing side effects. Unlike the uptake of naked siRNA dependent on the TLR3 pathway, the mechanisms of siRNA cellular uptake that form complexes with delivery systems are diverse. For example, lipid nanoparticles exhibit low-density lipid protein receptor-dependent cellular uptake[25], whereas most other nanoparticles show clathrin-mediated endocytosis or micropinocytosis[26,27]. The siRNA silencing effects *in vitro* and *in vivo* showed that PACD/siVEGFA induced target gene silencing in a strictly sequence-dependent manner (Figs. 3E and F, 6E and F) without eliciting immune response (Figs. 6D and 7C, Supporting Information Fig. S9). We suggest that the specific modification of the siRNA sequence combined with the efficient PACD polymeric micelle delivery system is responsible for the high gene silencing potency of the polyplexes. Our study once again highlights the importance of the rational design of siRNA drugs and their delivery systems.

4. Conclusions

In this work, we designed and synthesized a triblock copolymer PACD consisting of a pH-sensitive core block, a nucleic acid binding block and a hydrophilic block. Here, PACDs can easily self-assemble into supramolecular nanomicelles and deliver siRNA into retinal cells. Due to the pH-responsive nature of PACD, the PACD/siRNA polyplexes exhibit sensitive responses to acidic endosomes, inducing robust siRNA endosomal escape efficiency and superior gene silencing efficiency both *in vitro* and *in vivo*. With benefits from the hydrophilic shell, small size and slightly positive charge, the PACD/siRNA polyplexes can overcome the intraocular clearance mechanisms effectively after a single injection, rapidly distribute in all layers of the retina, and retain in the retina for more than one week upon single injection. Furthermore, the PACD/siVEGFA polyplexes abrogated the hypoxia-induced angiogenesis in an OIR mouse model without causing any inflammatory or histopathological changes. Our study provides some technical references and a theoretical basis for the rational design of an ocular gene delivery system.

Acknowledgments

This work was supported by the National Natural Science Foundation (32001008, 32171394, 31901053, 32101157, 32101148, 82202338, China), the National Key Research & Development Program of China (2021YFA1201000, 2021YFE0106900, 2021YFC2302400), the Fundamental Research Funds for the Central Universities (2022CX01013, China), Beijing Nova Program (Interdisciplinary Cooperation Project) from Beijing Municipal Science & Technology Commission (20220484207, China). We appreciate the kind suggestions and help from Prof. Bailiang Wang of Wenzhou Medical University. We thank the Biological and Medical Engineering Core Facilities, and Analysis & Testing Center, Beijing Institute of Technology for supporting experimental equipment, and staffs for valuable help with technical support.

Author contributions

Yuhua Weng, Xing-Jie Liang and Yuanyu Huang designed the research. Shuai Guo and Chunhui Li carried out the experiments and performed data analysis. Changrong Wang, Xiaowen Cao and Xinyue Liu participated part of the experiments. Yuhua Weng wrote the manuscript. Shuai Guo and Chunhui Li revised the manuscript. All of the authors have read and approved the final manuscript.

Conflicts of interest

The authors have no conflicts of interest to declare.

Appendix A. Supporting information

Supporting data to this article can be found online at https://doi.org/10.1016/j.apsb.2023.09.001.

References

1. Holmgaard AB, Askou AL, Jensen EG, Alsing S, Bak RO, Mikkelsen JG, et al. Targeted knockout of the *VEGFA* gene in the retina by subretinal injection of RNP complexes containing Cas9 protein and modified sgRNAs. *Mol Ther* 2021;**29**:191−207.
2. Koo T, Park SW, Jo DH, Kim D, Kim JH, Cho HY, et al. CRISPR-LbCpf1 prevents choroidal neovascularization in a mouse model of age-related macular degeneration. *Nat Commun* 2018;**9**:1855.

3. Weng YH, Xiao HH, Zhang JC, Liang XJ, Huang YY. RNAi therapeutic and its innovative biotechnological evolution. *Biotechnol Adv* 2019;**37**:801−25.
4. Migliorati JM, Jin J, Zhong XB. siRNA drug Leqvio (inclisiran) to lower cholesterol. *Trends Pharmacol Sci* 2022;**43**:455−6.
5. Hu B, Zhong LP, Weng YH, Peng L, Huang YY, Zhao YX, et al. Therapeutic siRNA: state of the art. *Signal Transduct Targeted Ther* 2020;**5**:101.
6. Del Amo EM, Urtti A. Current and future ophthalmic drug delivery systems. A shift to the posterior segment. *Drug Discov Today* 2008;**13**: 135−43.
7. Tan GX, Liu DD, Zhu RF, Pan H, Li JY, Pan WS. A core-shell nanoplatform as a nonviral vector for targeted delivery of genes to the retina. *Acta Biomater* 2021;**134**:605−20.
8. Gilleron J, Querbes W, Zeigerer A, Borodovsky A, Marsico G, Schubert U, et al. Image-based analysis of lipid nanoparticle-mediated siRNA delivery, intracellular trafficking and endosomal escape. *Nat Biotechnol* 2013;**31**:638−46.
9. Gong NQ, Zhang YX, Teng XC, Wang YC, Huo SD, Qing GC, et al. Proton-driven transformable nanovaccine for cancer immunotherapy. *Nat Nanotechnol* 2020;**15**:1053−64.
10. Li CH, Zhou JH, Wu YD, Dong Y, Du LL, Yang TR, et al. Core role of hydrophobic core of polymeric nanomicelle in endosomal escape of siRNA. *Nano Lett* 2021;**21**:3680−9.
11. Wojnilowicz M, Glab A, Bertucci A, Caruso F, Cavalieri F. Super-resolution imaging of proton sponge-triggered rupture of endosomes and cytosolic release of small interfering RNA. *ACS Nano* 2019;**13**:187−202.
12. Guo S, Li K, Hu B, Li CH, Zhang MJ, Hussain A, et al. Membrane-destabilizing ionizable lipid empowered imaging-guided siRNA delivery and cancer treatment. *Explorations* 2021;**1**:35−49.
13. Zhang TB, Huang YY, Ma XW, Gong NQ, Liu XL, Liu L, et al. Fluorinated oligoethylenimine nanoassemblies for efficient siRNA-mediated gene silencing in serum-containing media by effective endosomal escape. *Nano Lett* 2018;**18**:6301−11.
14. Kang HC, Bae YH. pH-Tunable endosomolytic oligomers for enhanced nucleic acid delivery. *Adv Funct Mater* 2007;**17**:1263−72.
15. Yu TZ, Liu XX, Bolcato-Bellemin AL, Wang Y, Liu C, Erbacher P, et al. An amphiphilic dendrimer for effective delivery of small interfering RNA and gene silencing *in vitro* and *in vivo*. *Angew Chem Int Ed Engl* 2012;**51**:8478−84.
16. Huang XG, Zhou GH, Wu WY, Duan YJ, Ma GE, Song JY, et al. Genome editing abrogates angiogenesis *in vivo*. *Nat Commun* 2017;**8**:112.
17. Patel P, Ibrahim NM, Cheng K. The importance of apparent pK_a in the development of nanoparticles encapsulating siRNA and mRNA. *Trends Pharmacol Sci* 2021;**42**:448−60.
18. Jayaraman M, Ansell SM, Mui BL, Tam YK, Chen J, Du X, et al. Maximizing the potency of siRNA lipid nanoparticles for hepatic gene silencing *in vivo*. *Angew Chem Int Ed Engl* 2012;**51**: 8529−33.
19. Campochiaro PA. Molecular pathogenesis of retinal and choroidal vascular diseases. *Prog Retin Eye Res* 2015;**49**:67−81.
20. Xu QG, Boylan NJ, Suk JS, Wang YY, Nance EA, Yang JC, et al. Nanoparticle diffusion in, and microrheology of, the bovine vitreous *ex vivo*. *J Control Release* 2013;**167**:76−84.
21. Veleri S, Lazar CH, Chang B, Sieving PA, Banin E, Swaroop A. Biology and therapy of inherited retinal degenerative disease: insights from mouse models. *Dis Model Mech* 2015;**8**:109−29.
22. Pitkänen L, Ruponen M, Nieminen J, Urtti A. Vitreous is a barrier in nonviral gene transfer by cationic lipids and polymers. *Pharm Res (N Y)* 2003;**20**:576.
23. Chappelow AV, Kaiser PK. Neovascular age-related macular degeneration: potential therapies. *Drugs* 2008;**68**:1029.36a.
24. Kleinman ME, Yamada K, Takeda A, Chandrasekaran V, Nozaki M, Baffi JZ, et al. Sequence- and target-independent angiogenesis suppression by siRNA *via* TLR3. *Nature* 2008;**452**:591−7.
25. Akinc A, Querbes W, De S, Qin J, Frank-Kamenetsky M, Jayaprakash KN, et al. Targeted delivery of RNAi therapeutics with endogenous and exogenous ligand-based mechanisms. *Mol Ther* 2010; **18**:1357−64.
26. Means N, Elechalawar CK, Chen WR, Bhattacharya R, Mukherjee P. Revealing macropinocytosis using nanoparticles. *Mol Aspect Med* 2022;**83**:100993.
27. Canton I, Battaglia G. Endocytosis at the nanoscale. *Chem Soc Rev* 2012;**41**:2718−39.